PAPER

3-D self-assembly of flower-like particles *via* microwave irradiation for water treatment

Youngsoo Jung, You-Hwan Son and Jung-Kun Lee*

Three-dimensional (3-D) flower-like shape (FLS) Fe_3O_4 and Fe particles were successfully synthesized using FLS precursor particles that are prepared through a facile microwave-assisted reaction. The mechanism underlying the self-assembly process and shape evolution of FLS particles was systematically investigated by changing reaction parameters such as reaction temperature, reaction time and reaction pressure. During the reaction, iron alkoxide, α-Fe_2O_3 and FeOOH nanoparticles are formed first and are subsequently transformed to 3-D hierarchical FLS particles by the self-assembly of the primary nanoparticles. Reaction temperature and pressure play critical roles in the formation of the hierarchical flower-like superstructure. There is an optimum window of the reaction temperature (~ 180 °C) for the formation of 3-D FLS particles, which is attributed to the competition between the self-assembly process and growth process of the nanoparticles. Also, since $FeCl_3$, ethylene glycol, and urea are used together as raw materials, the appearance of FLS particles is strongly dependent on the reaction pressure. As the reaction pressure becomes larger than 1 MPa, the flake type particles become more thermodynamically favorable than the FLS particles, due to the limited decomposition of urea. Brunauer–Emmett–Teller (BET) analysis shows that FLS particles have a large surface area (>40 m^2 g^{-1}). Because of their high specific surface area and intrinsic reactivity, FLS particles efficiently remove sulfur ions in aqueous solution. This suggests that these flower-like particles can be promising materials to treat toxic gas such as H_2S in an environment-friendly way.

Introduction

Synthesis of intricate 3-dimensional (3D) hierarchical nanostructure materials with controlled morphology and orientation has attracted intense interest owing to their potential application in catalysis, drug delivery, energy storage, water treatment, and sensors.[1–15] Many kinds of hierarchical superstructured materials such as nano-flowers, snowflakes, and dendrites have been successfully synthesized and examined to explore their physical and chemical characteristics with respect to morphology.[16–18] In general, the simplest synthetic route to a 3-dimensional hierarchical structure is the oriented assembly of nanoparticles to decrease their surface energy by stacking nanoparticle building blocks. Therefore, it is important to develop simple and reliable synthetic methods for hierarchically ordered architectures with desired morphology, which greatly acts on the properties of the final product.

Recently, a microwave reaction has been applied to chemically synthesize nanomaterials. This technique offers several advantages over other conventional techniques, such as vapor–liquid–solid (VLS), vapor phase, hydrothermal and solvothermal synthesis.[19–22] Microwave irradiation reduces reaction time and

Department of Mechanical Engineering & Material Science, University of Pittsburgh, Pittsburgh, PA, 15261. E-mail: jul37@pitt.edu

temperature, which is due to the molecular level interaction of the microwave with the reagent species.[23,24] This has allowed the preparation of highly crystalline nanomaterials with tailored shapes and sizes, such as uniform Ag nanoparticles, microporous SnO_2, TiO_2 nanowires, CdTe nanocrystals, Cu_3Se_2 nanoplates, and iron oxide nanorings.[25–30]

Fe-based magnetic nanomaterials have been intensively studied for applications of magnetic data storage devices, magnetic resonance imaging, biomedical markers, wireless sensors, water treatments, and ferrofluids.[31–40] In addition to their outstanding magnetic properties, a very unique intrinsic property of Fe-based nanomaterials is their sulfidation ability. Fe-based materials are easily converted to iron sulfide, which is used to decompose hydrogen sulfide (H_2S). Due to its toxic and flammable nature, H_2S needs to be removed from waste gas streams of chemical plants or from byproducts of oil/gas drilling operations.[41,42] Various transition metal oxide materials with high catalytic activity have been utilized in H_2S removal.[43–45] Among these materials, Fe-based materials are widely reported as strong oxidation reagents for H_2S treatment.[46,47]

Several methods have been developed to synthesize Fe_3O_4 and Fe particles, which include thermal decomposition, co-precipitation, hydrothermal processing, reverse micelle, and sol–gel processing.[48–52] In comparison, the effect of microwaves on the

growth of Fe_3O_4 and Fe particles with a hierarchical super-structure has not been studied yet. Herein, we demonstrate a facile microwave-assisted method to fabricate flower-like Fe_3O_4 and Fe particles. The effect of reaction parameters and annealing conditions on the morphology and phase of the particles were examined. A growth mechanism of hierarchical particles in ethylene glycol (EG)-mediated solution was proposed. Moreover, the reaction of flower-like particles with S^{2-} ions was tested to evaluate their efficacy as a H_2S absorbent in water.

Experimental section

Synthesis of flower-like shape particles

The fabrication of flower like shape (FLS) iron oxide particles was achieved by the ethylene glycol (EG) mediated self-assembly process of nanoparticles, which has been adapted to the synthesis of several nanomaterials.[53–55] 1.3 g of $FeCl_3 \cdot 6H_2O$, 7.2 g of tetrabutylammonium (TBAB), and 2.7 g of $CO(NH_2)_2$ (urea) were mixed homogeneously in 180 ml of EG at room temperature for 1 h. A mixture precursor with a red color was loaded into a Teflon vessel. The solution in a sealed Teflon vessel was reacted at 120–210 °C for 30 min under microwave irradiation (CEM-Marsxpress, USA). Pressure inside the vessel was controlled to be between 0.2 MPa and 1 MPa. Reaction temperature and pressure were independently controlled by changing the input of microwave power and the solution content in the vessel. The resulting particles were collected by centrifugation, washed out with ethanol several times and subsequently dried in a vacuum oven at room temperature for 18 h. As-grown particles with green color were crystallized at 400 °C in N_2 or forming gas ($N_2 + 5\%H_2$) for 2 h.

Sample characterization

The crystal structure of the thermally-annealed FLS-iron oxide particles was examined by the X-ray diffraction (XRD) method (Philips, PW-1810 diffractometer, Cu-Kα radiation, $\lambda = 1.54$ Å). The Raman spectroscopy of particles was carried out at room temperature with an incident beam wavelength of 633 nm (Renishaw, inVia Raman microscope). The Fourier transform infrared (FTIR, Bruker VERTEX-70LS) spectra was recorded in a transmission geometry. Particles were mixed with KBr and the mixed particles were pressed into to pellets. The morphology of FLS iron oxide particles was probed by field emission-scanning electron microscope (FE-SEM, Philips XL-30) and transmission electron microscope (TEM, JEOL 200CX). Magnetic properties were measured at room temperature by vibrating sample magnetometer (VSM, Lake Shore 7400). Nitrogen adsorption and desorption isotherm of the particles were also measured at liquid nitrogen temperature to analyze the surface structure. Before the adsorption measurement, the samples were outgassed under vacuum for 3 h at 100 °C. In order to confirm the sulfidation ability of FLS particles, 0.1 g of the particles was introduced into 100 ml of 12.5 mM sodium sulfide (Na_2S) aqueous solution in a 200 ml glass. Then, the concentration of sulfur ion in water was monitored by measuring the ionic conductivity of S^{2-} (Denver instrument, 250 conductivity meter) at every 10 min.
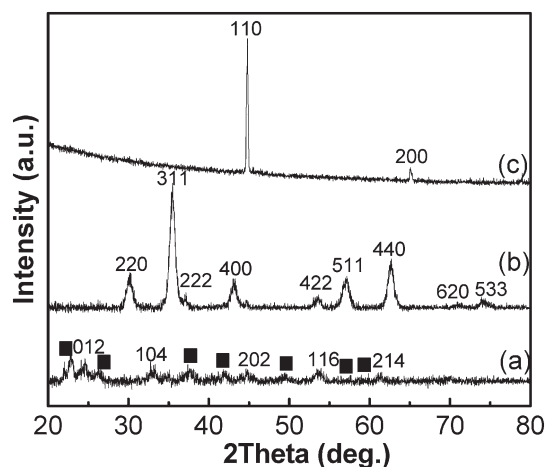

Fig. 1 XRD patterns of fabricated FLS particles; (a) as-grown FLS-precursor, (b) FLS–Fe_3O_4, and (c) FLS–Fe particles. (■ : α-FeOOH)

Results and discussion

Crystal structure analyses

XRD patterns of the as-grown and annealed particles are presented in Fig. 1. In the XRD pattern of the as-grown FLS-precursor particles (Fig. 1a), broad peaks indicate a co-existence of α-Fe_2O_3 and α-FeOOH. Nucleation of α-FeOOH is known to compete with that of α-Fe_2O_3 below 80 °C.[56] Reflections of the as-grown particles at 26.4°, 33.0°, 44.8°, 53.7°, and 61.3° are indexed as (012), (104), (202), (116), and (214) of α-Fe_2O_3 (JCPDS 80-2377). Fig. 1(b) and Fig. 1(c) show XRD patterns of the samples that were annealed at N_2 and $N_2+5\%H_2$ atmosphere. To make the particles magnetically active, particles were annealed only in a reducing atmosphere. After being annealed at 400 °C in a N_2 atmosphere, the XRD pattern of the FLS particles matches well with the diffraction pattern of Fe_3O_4 (magnetite, JCPDS 85-1436). In comparison, annealing in $N_2+5\%H_2$ resulted in the appearance of an Fe phase (JCPDS 87-0721).

There are several polymorphs of iron oxide and oxyhydroxide (e.g., α-Fe_2O_3, α-FeOOH, γ-FeOOH) and each phase exhibits a distinctive Raman spectrum. The Raman investigation, therefore, is regarded as one of the reliable methods to discern phases of the particles which do not have a long range order.[58] In addition, Raman spectroscopy is complementary to XRD analysis, which does not differentiate Fe_3O_4 from γ-Fe_2O_3 clearly.[59] To accurately identify the crystal phase of each product, Raman spectroscopy is used and the Raman spectra of the as-grown and N_2-annealed particles are displayed in Fig. 2. For the as-grown precursor particles (Fig. 2a), Raman peaks represent the coexistence of α-FeOOH (227, 262, 324, and 432 cm^{-1}) and α-Fe_2O_3 phases (388, 494, 616, 652, 826, 914, 1064, and 1103 cm^{-1}), which are in agreement with reported studies.[60–62] The Raman spectra of N_2-annealed FLS particles are presented in Fig. 2b. A relatively strong band centered at 661 cm^{-1} and two broad peaks at 306, and 530 cm^{-1} exhibit in the results, confirming the formation of the Fe_3O_4 phase for FLS–Fe_3O_4 particles.[63,64] This indicates that the as-grown particles consisting of α-Fe_2O_3 and α-FeOOH phases are fully transformed to Fe_3O_4 in N_2-annealing.
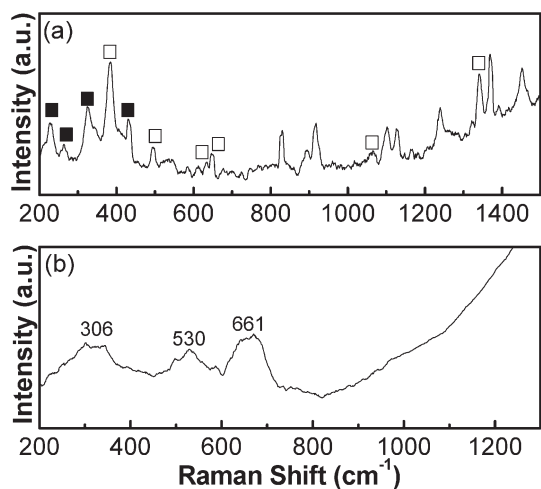
Fig. 2 Raman spectra of (a) as-grown FLS particles and (b) N_2-annealed FLS particles ($\blacksquare$ = α-FeOOH, $\square$ = α-Fe_2O_3).

When $FeCl_3$ meets with EG, a series of reactions occur and nanoparticles are formed in the precursor solution. First, $FeCl_3$ first meets with EG (HOC_2H_4OH) and a partial reduction occurs to generate iron alkoxide.[57] Then, Fe_2O_3 primary nanoparticles are formed by a reaction between iron alkoxide and oxygen.[22] In addition to the precipitation of Fe_2O_3 nanoparticles, Fe^{3+} from $FeCl_3$ can directly react with OH^- and produce FeOOH. To validate the reaction mechanism of primary nanoparticles, the FTIR spectra of the as-grown and thermally-annealed FLS particles were investigated. The FTIR spectrum of the as-grown FLS particles is shown in Fig. 3. The strong absorption band lying in the 2500–3000 cm^{-1} range is characteristic of the C–H stretching mode and all the peaks located below 1750 cm^{-1} are Fe–O, C–O, C–C, and CH_2 bonds that are the main moieties of Fe-alkoxide.[65] With Raman spectra and XRD patterns, the FTIR spectra clearly supports that the Fe-alkoxide is formed from the EG-mediated reaction of $FeCl_3$ and a significant amount of Fe-alkoxide is still left in the as-grown particles.
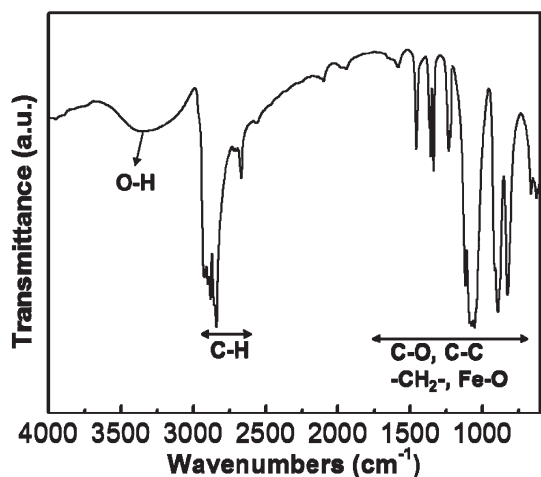

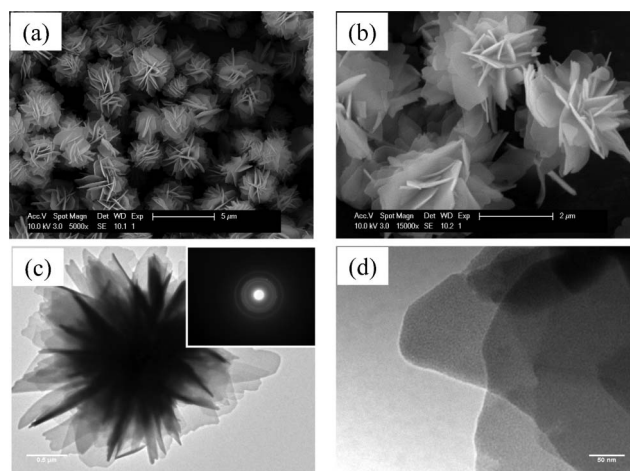**Fig. 3** FTIR spectra of the as-grown FLS particles.

Fig. 4 SEM and TEM micrographs of as-grown FLS-precursor particles. (Inset: selected area diffraction (SAD) patterns.)

Morphology of the superstructured particles

Changes in the morphological characteristics were examined by SEM and TEM. Fig. 4 shows SEM and TEM micrographs of the as-grown FLS particles. When raw materials were reacted at 180 °C and below 0.2 MPa, the product of the reaction was FLS particles with a size of 2∼3 µm. The surface of the petal-like plates was very smooth and their thickness was smaller than 100 nm (Fig. 4a and 4b). A detailed microstructure of FLS particles is shown in the inset of Fig. 4c. The selected area diffraction (SAD) patterns of as-grown FLS-particles exhibit diffraction rings confirming polycrystalline nature of the as-grown FLS particles. This is consistent with XRD patterns. Grain boundaries of nanoparticles are not observed even in a TEM micrograph with higher magnification (Fig. 3d). Fig. 5 shows SEM and TEM micrographs of the particles after thermal annealing. The morphology of Fe_3O_4 nanoparticles crystallized by N_2 annealing is similar to that of as-grown FLS particles (Fig. 5a). This suggests that FLS particles maintain their unique shape during N_2 treatment at 400 °C. TEM images of Fe_3O_4 (Fig. 5b and 5c) indicate that each petal-like plate of FLS particles is polycrystalline and porous. Appearance of pores in the petals of FLS particles is ascribed to the decomposition of iron alkoxide and α-FeOOH and the removal of residual organic species during annealing. The SAD patterns (the inset of Fig. 5b) clearly reveal polycrystalline nature. High magnification TEM micrograph in Fig. 5c shows that the individual petal consists of small nanoparticles with a size of 10∼15 nm. This value is in consistent with the particle size that is determined by analyzing XRD patterns *via* Debye-Scherrer equation. In comparison, Fe particles crystallized by N_2+5%H_2 annealing display a moderate change in the shape during the annealing process (Fig. 5d). Though the hierarchical superstructure was found and the pores were created, FLS particles partially collapsed and the petals warped more after N_2+5%H_2 annealing than N_2 annealing.

Effects of reaction parameters on primary particles and self-assembly

The morphology of the superstructured particles is sensitive to experimental parameters such as reaction temperature, reaction
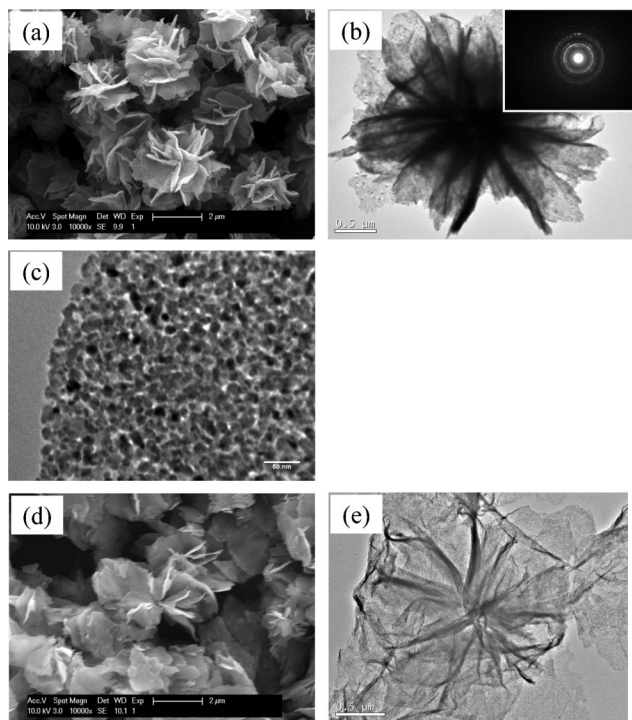
Fig. 5 SEM and TEM micrographs of (a), (b), (c) FLS–Fe$_3$O$_4$ and (d), (e) FLS–Fe particles. (Inset: selected area diffraction (SAD) patterns of FLS–Fe$_3$O$_4$ particles.)

time, reagent concentration, solvent types, and solution pH.[66–68] In the present work, we systematically investigated the evolution of the hierarchical structures during the microwave-assisted reaction. There is an optimum range of reaction temperature and reaction pressure, which is suitable for the formation of hierarchically structured FLS-particles. Among the experimental variables, the reaction temperature is critical in the self-assembly of the nanoparticles. As shown in Fig. 6a, the reaction at 120 °C leads to irregular aggregates of nanoparticles. When the reaction temperature was increased to 150 °C (Fig. 6b), the nanoparticles assemble to form 3-dimensional (3-D) frameworks of nano-
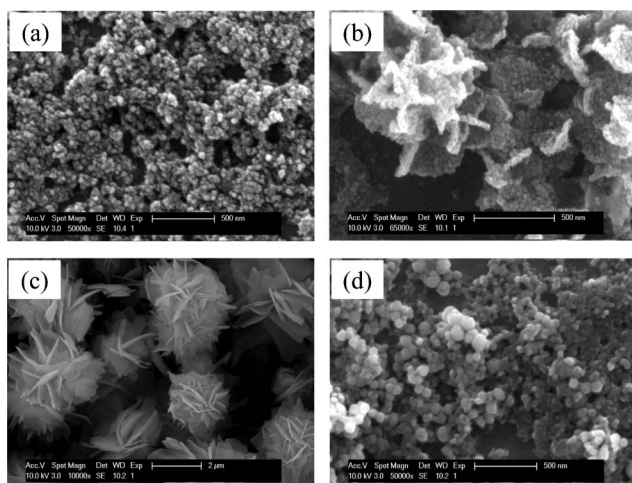

Fig. 6 SEM micrographs of the as-grown particles obtained at different reaction temperatures; (a) 120 °C, (b) 150 °C, (c) 180 °C, and (d) 210 °C.

plates. However, the binding strength between the nanoplates is not strong enough to make the surface of the nanoplates smooth. The surface is rough and the individual nanoparticle are still identified. At the reaction temperature of 180 °C (Fig. 6c), the 3-D hierarchical architecture with a very smooth surface is achieved. However, further increase of the reaction temperature to 210 °C (Fig. 6d) results in random aggregates of nanoparticles with diameters of 90–100 nm. Self-assembly of the nanoparticles is not observed. This implies that the self-assembly process of the nanoparticles competes with the growth process of the nano-particles and that there is an optimum window of the reaction temperature for the formation of 3-D FLS particles.

The other parameter that was examined in this study is the reaction pressure. Since the precursors were reacted in a sealed Teflon vessel, the increase in the reaction temperature is accompanied by the increase in the reaction pressure. To separate the effect of the reaction temperature from that of the reaction pressure, the reaction temperature was fixed at 180 °C and only the reaction pressure was controlled by varying the volume of the precursor solution inside a sealed Teflon reactor. SEM micrographs in Fig. 7 show the change in the morphology of the reaction products as a function of the pressure. When the pressure in the reactor is below 0.2 MPa (Fig. 7a), well-structured hierarchical FLS particles were obtained. While, when the pressure was between 0.3 and 1 MPa (Fig. 7b), the petal-like plates consisting of the nanoparticles were observed. A part of the particles have the microstructure of stacked plates and a part of them show the 3-D FLS structure. When the pressure was higher than 1 MPa (Fig. 7c), the particles turned to large flakes. The change from the FLS structure to the flake structure is explained by the role of urea. In the EG-mediated reaction of FeCl$_3$, HCl is produced as a byproduct.[69] However, an increase in HCl concentration decreases pH and prohibits further conversion of FeCl$_3$ to the iron alkoxide. This, in turn, decreases the yield of the EG-mediated reaction. To prevent the side effect of HCl, urea is added to the precursor solution as a neutralizing agent that is decomposed to provide counter ions, OH$^-$. In the previous study, Chen *et al.* suggested that the decomposition of urea is sensitive to the pressure of a reaction solution.[70]

$$CO(NH_2)_2 \rightarrow NH_4^+ + CON^- \ (T \geqslant 80\ °C) \qquad (1)$$

$$CON^- + 3H_2O \rightarrow NH_4^+ + 2OH^- + CO_2 \qquad (2)$$
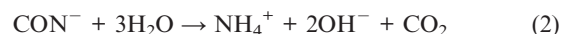
As described in eqn (1) and (2), the decomposition of urea releases CO$_2$ gas as well as OH$^-$ ions. Therefore, the increase in the reaction pressure restricts the decomposition of urea by preventing the release of CO$_2$ from the solution. The urea decomposition starts to be limited at the pressure of 0.5 MPa. When the reaction pressure reaches 0.9 MPa, only a small portion of urea is decomposed. This indicates that the conversion of FeCl$_3$ to iron alkoxide is negligible at high pressure and the amount of primary nanoparticles from iron alkoxide is not large enough to develop the 3-D hierarchical superstructure. As a result, only 2-D flake type particles are produced in the high pressure environment.

Mechanism of the self-assembly of 3-D FLS particles

To understand the self-assembly process of 3-D FLS particles, the reaction process was monitored as a function of reaction
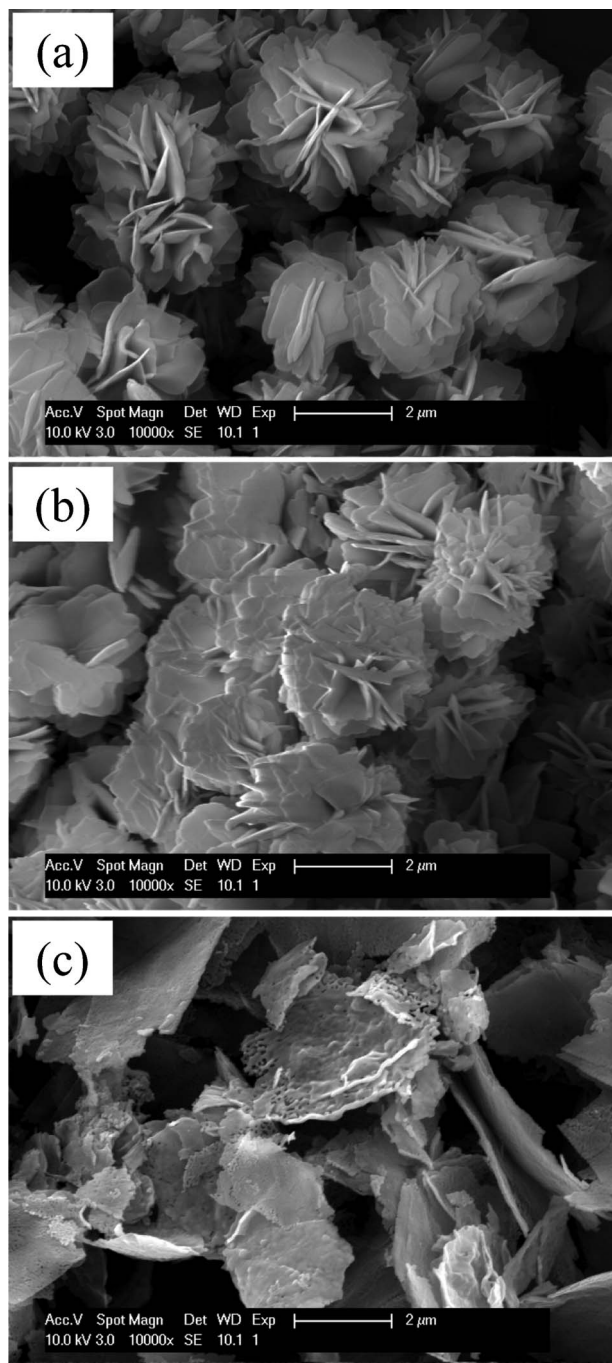
Fig. 7 Change in the morphology of the reaction products as a function of the pressure; (a) $\sim$0.2 MPa, (b) 0.3 $\sim$ 1 MPa, and (c) 1 MPa.

Fig. 8 SEM micrographs of as-grown particles as a function of reaction time; (a) 20 s, (b) 60 s, (c) 2 min, and (d) 5 min (a scale bar in the inset is 1 μm).

turn to fully developed FLS particles, as shown in Fig. 8d. From this point, the morphology and size of FLS particles were maintained. It is worth noting that the growth of fully developed FLS particles under the microwave irradiation was completed within 5 min, which is much faster than conventional methods. This means that the 'hot-spots' effects induced by the microwave irradiation may create an environment suitable for the fast nucleation of nanoparticles and their accelerated growth to FLS-precursor particles.[71]

On the basis of experimental observations in the above, a three-step growth mechanism is proposed. This is composed of i) a fast nucleation of amorphous primary nanoparticles, ii) an aggregation of nanoparticles into the microspheres with rough surface, and iii) the self-assembly of thin plates onto the microspheres.[72–74] Oriented assembly of the nanoparticles has been considered as a key step in producing the hierarchical superstructure.[75] Various factors influence the oriented assembly of the nanoparticles, such as surface energy, electrostatic and dipolar fields, van der Waals forces, hydrophobic interactions, and hydrogen bonds. Given that the surfactants are not added to the precursor solution in this study, the surface energy is speculated to play a major role in the formation of FLS particles. Penn *et al.* and Li *et al.* propose that a main driving force to develop such hierarchical particles is a tendency to reduce the high surface energy *via* self-assembly of adjacent particles.[76,77] In addition, the chelating ability of EG may contribute to the formation of FLS particles. Li *et al.* suggests that the generation of self-assembly of nanosheets is caused by the anchored polyol molecules. The strong chelating ability of the EG with iron ions makes it anchor to the surface and edges of nanosheets.[78] This gives rise to edge-to-edge attachment and edge-to-surface conjunction among the nanoparticles, leading to the formation of hierarchical FLS superstructure.

Magnetic property of FLS oxide particles

Magnetization is one of the important parameters to evaluate the structure and property of Fe-based materials.[79] To investigate the magnetic properties of the FLS–Fe_3O_4 and Fe particles, the

time. As seen in Fig. 8a, the product at the early stage of the reaction, at 180 °C and below 0.2 MPa, was nanoparticles with a diameter of about 50 nm. A large amount of the nanoparticles was formed within 20 s in the precursor solution. After the microwave-assisted reaction continued for 1 min (Fig. 8b), a small portion of the nanoparticle gather to form microspheres with a diameter of 1-2 μm. The microspheres coexist with the nanoparticles. As the reaction proceeded (Fig. 8c), most of the nanoparticles is consumed to form the microspheres. Simultaneously, 3-D hierarchical structures started to appear. When the reaction time continued for 5 min, all nanoparticles
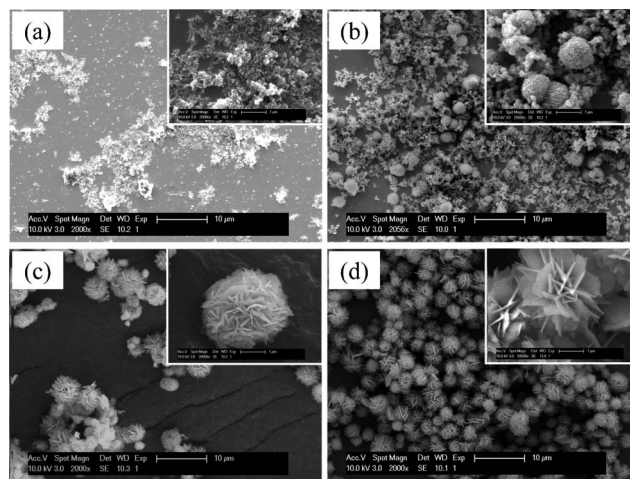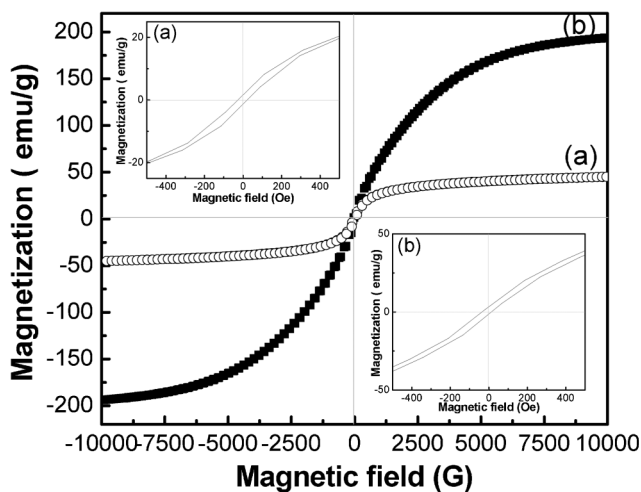
Fig. 9 Magnetic hysteresis loops of (a) FLS–Fe$_3$O$_4$ and (b) FLS–Fe particles.

magnetic properties of the particles were measured at room temperature using VSM. M–H curves are shown in Fig. 9. The saturation magnetization (M_s) of the FLS–Fe$_3$O$_4$ particles (Fig. 9a) was 45.0 emu g^{-1}. The inset (a) of Fig. 9 shows that the coercivity (H_c) for the Fe$_3$O$_4$ was 23.6 Oe. The M_s value for FLS–Fe$_3$O$_4$ was lower than the value of bulk Fe$_3$O$_4$ (92 emu g^{-1}). This is attributed to the non-stoichiometric defects in Fe$_3$O$_4$ which discontinue superexchange bonds among Fe cations.[80] In contrast, M_s of FLS–Fe particles (Fig. 9b) was about 193.8 emu g^{-1}, and the H_c value was about 23.6 Oe (Fig. 9, inset (b)). FLS-Fe particles had slightly lower M_s than bulk Fe (217.6 emu g^{-1}). This small difference in saturated magnetizations between FLS–Fe particles and Fe bulk indicates that the shape anisotropy and the surface pinning do not have a significant impact on the magnetic properties of the petal-like plates in FLS particles.

Surface characteristics

Fig. 10 shows the nitrogen adsorption–desorption isotherms and corresponding pore size distribution of as-grown particles, Fe$_3$O$_4$ and Fe particles, respectively. The Brunauer–Emmett–Teller (BET) surface area of as-grown FLS particles (Fig. 10a) was 15.7 m^2 g^{-1}, while the FLS–Fe$_3$O$_4$ (Fig. 10b) and FLS–Fe (Fig. 10c) particles had specific surface areas of 71.1 m^2 g^{-1} and 41.9 m^2 g^{-1}, respectively. The increased surface area of thermally-annealed FLS particles is attributed to the formation of internal pores. The adsorption and desorption isotherms of the as-grown particles in Fig. 10a are close to type II isotherms that do not show the hysteresis loop. Given that the type II isotherm is typical for non-porous or macroporous materials, the isotherms in Fig. 10a indicate that the as-grown FLS particles do not have mesopores.[81] In contrast, the isotherms of thermally-annealed FLS particles (Fe$_3$O$_4$ and Fe) exhibit the hysteresis loops that result from different adsorption and desorption in the mesopores. The isotherm of FLS–Fe$_3$O$_4$ displays the features of H3 type hysteresis loops. This indicates that both slit-like mesopores and micropores are formed during the annealing. The coexistence of mesopores and micropores is confirmed in the pore size distribution curve, shown in the inset of Fig. 10b.
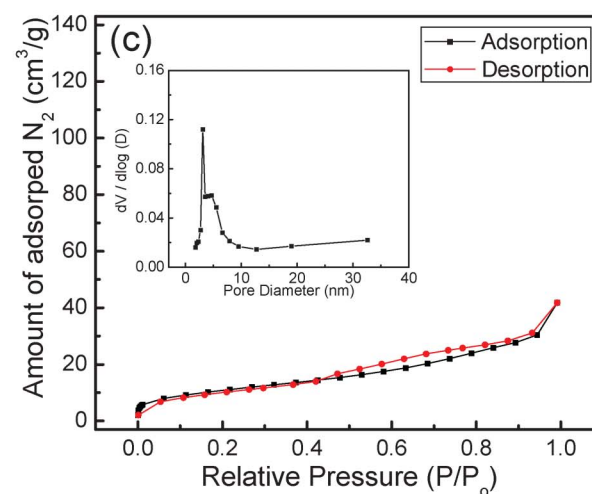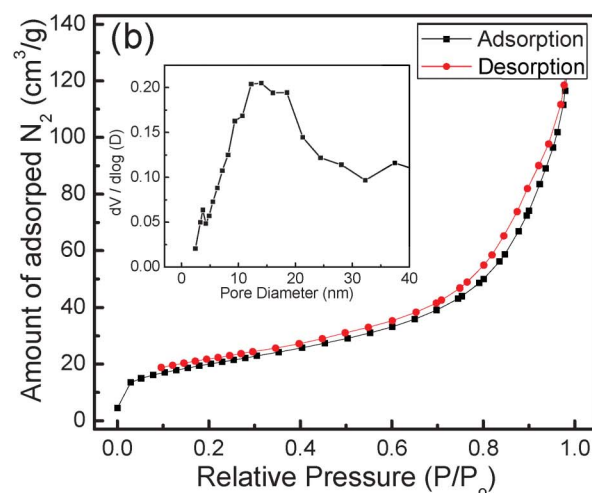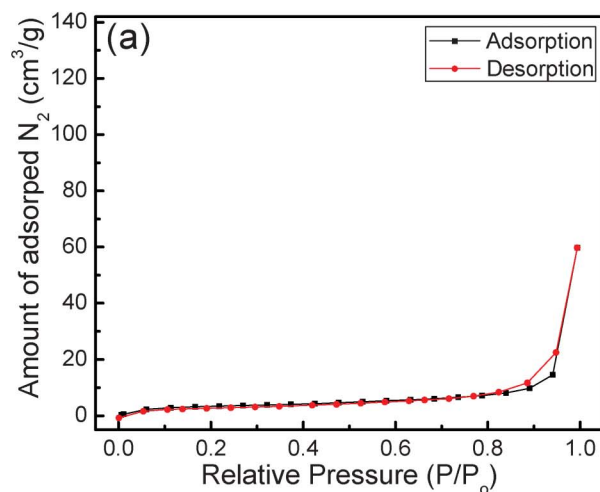

Fig. 10 Nitrogen adsorptioin–desorption isotherms and pore size distribution curves of (a) as-grown FLS-precursor, (b) FLS–Fe$_3$O$_4$, and (c) FLS–Fe particles. (Inset: pore size distribution curve.)

Though the hysteresis loop is also observed, the isotherm curve of FLS–Fe particles is close to H4 type hysteresis loop in that the adsorption and desorption branches remain nearly horizontal over a wide range of p/p_o. This H4 type hysteresis loop shows

that the phase transition to metallic Fe during the annealing in reducing environment develops the slit-like mesopores with a well-defined size and shape. The results of the BET analysis are consistent with TEM micrographs of Fig. 5, showing that the decomposition of iron alkoxide and α-FeOOH and the removal of organic species during the thermal annealing create mesopores in the FLS–Fe$_3$O$_4$ and FLS–Fe particles. The large surface area of thermally-annealed FLS particles suggests that these hierarchical structured particles would be utilized as efficient catalysts and absorbents.

Application to water treatment

Hydrogen sulfide (H$_2$S) has been reported as a malodorous toxic gas which could spread out through water.[82] To remove H$_2$S from water, several sorbents containing metal elements such as Fe, Zn, Ti, V, and Al, have been intensively explored.[46,83–85] In this study, we tested the capability of FLS particles to remove H$_2$S from water. To simulate H$_2$S dissolved in water, Na$_2$S was added to water. When sodium sulfide (Na$_2$S) is exposed to moist environment, Na$_2$S and its hydrates emit hydrogen sulfide. In the solution, as summarized in eqn (3), the dianion S^{2-} does not exist in perceivable amounts in water since S^{2-} is excessively strong base which may not be favorable for coexistence with water. Dissolution of Na$_2$S in the water is expressed as follow:

$$Na_2S(s) + H_2O(l) \rightarrow 2Na^+ + HS^- + OH^- \qquad (3)$$
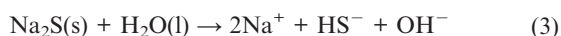
After FLS particles were added to the solution, the relative concentration of HS$^-$ in water was examined by measuring the electrical conductivity of the solution. Fig. 11 shows the concentration of sulfur ion as a function of reaction time. Both FLS–Fe$_3$O$_4$ and Fe removed most of the sulfur ions from the solution within 10 min. When the aqueous solution of 3000 ppm Na$_2$S was reacted for 50 min, less than 2% of the sulfur ions were left in solution. It is known that the reaction between Fe and S gives FeS$_2$ or Fe$_3$S$_4$, depending on their thermodynamic stability in the reaction conditions. Fast removal of H$_2$S, shown in Fig. 11, indicates that the large surface areas of the FLS–Fe and
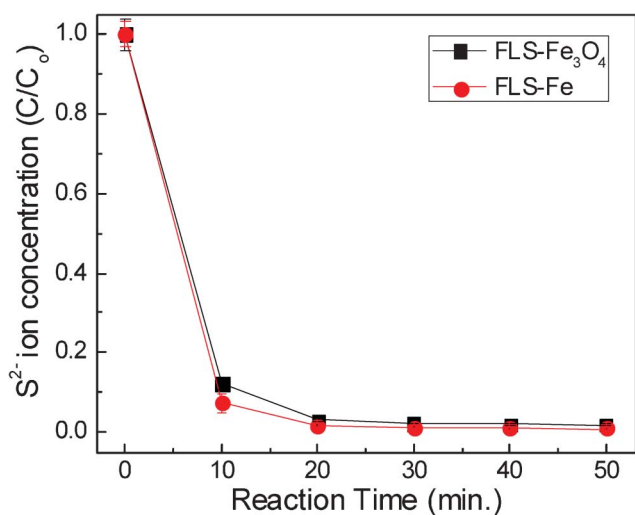
FLS–Fe$_3$O$_4$ particles provide plenty of active sites for the sulfidation reaction. Almost similar HS$^-$ removal rates by FLS–Fe and FLS–Fe$_3$O$_4$ particles imply that the activation energy for the reaction with HS$^-$ may be lower for Fe than for Fe$_3$O$_4$ and that the different reaction kinetics may compensate for the difference in surface area.

Conclusions

In this work, we have demonstrated the facile and fast synthesis of FLS–Fe$_3$O$_4$ and FLS–Fe particles. Hierarchical precursor particles have been successfully prepared by a microwave-assisted reaction of FeCl$_3$·6H$_2$O, TBAB, urea, and EG at 180 °C for 30 min. FLS particles with a hierarchical structure are formed through the self-assembly of iron alkoxide, α-Fe$_2$O$_3$ and FeOOH nanoparticles. The appearance of FLS particles is sensitive to reaction temperature and reaction pressure. Due to the competition between the self-assembly process and growth process of the nanoparticles, there is an optimum window of the reaction temperature for the formation of 3-D FLS particles. Also, the combined use of FeCl$_3$, EG, and urea as raw materials makes the reaction of FLS particles strongly dependent on the pressure. Since urea is not decomposed well at high pressure (>1 MPa), FLS particles are synthesized at pressures lower than 1 MPa. The surface area of the as-grown FLS particles is 15.7 m^2 g^{-1}, while the FLS–Fe$_3$O$_4$ and FLS–Fe particles exhibit specific surface areas of 71.1 m^2 g^{-1} and 41.9 m^2 g^{-1}, respectively. The decomposition of iron alkoxide, α-FeOOH and the removal of organic species during the thermal-annealing leaves micro- and mesopores in the FLS particles. Because of their high specific surface area, mesoporosity, and intrinsic reactivity, FLS–Fe$_3$O$_4$ and Fe particles exhibit an excellent ability to remove sulfur ions from aqueous solution. 0.1 g of both FLS–Fe$_3$O$_4$ and Fe remove most of the sulfur ions ($\sim$ 90%) in 12.5 mM Na$_2$S aqueous solution within 10 min. This suggests that the FLS particles are good absorbers of toxic H$_2$S in aqueous solution.

References

1 X. Song and L. Gao, *J. Phys. Chem. C*, 2008, **112**, 15299.
2 X. Fu, H. Feng and K. Ng, *Nanotechnology*, 2009, **20**, 375601.
3 S. K. Mohapatra, S. E. John, S. Banerjee and M. Misra, *Chem. Mater.*, 2009, **21**, 3048.
4 S. Liu, R. Xing, F. Lu, R. Rana and J. Zhu, *J. Phys. Chem. C*, 2009, **113**, 21042.
5 S. Guo, L. Wang and E. Wang, *Chem. Commun.*, 2007, 3163.
6 B. Liu and H. C. Zeng, *J. Am. Chem. Soc.*, 2004, **126**, 8124.
7 B. B. Kale, J. O. Baeg, S. M. Lee, H. Chang, S. J. Moon and C. W. Lee, *Adv. Funct. Mater.*, 2006, **16**, 1349.
8 Y. Hou, H. Kongdoh and T. Ohta, *Chem. Mater.*, 2005, **17**, 3994.
9 L. S. Zhong, J. S. Hu, H. P. Liang, A. M. Cao, W. G. Song and L. J. Wan, *Adv. Mater.*, 2006, **18**, 2426.
10 X. M. Sun, J. F. Liu and Y. D. Li, *Chem.–Eur. J.*, 2006, **12**, 2036.
11 J. Zhang, S. Wang, M. Xu, Y. Wang, B. Zhu, S. Zhang, W. Huang and S. Wu, *Cryst. Growth Des.*, 2009, **9**, 3532.
12 X. Yin, C. Li, M. Zhang, Q. Hao, S. Liu, Q. Li, L. Chen and T. Wang, *Nanotechnology*, 2009, **20**, 455503.
13 C. Li, L. Li, Z. Du, H. Yu, Y. Xiang, Y. Li, Y. Cai and T. Wang, *Nanotechnology*, 2008, **19**, 35501.

Fig. 11 Concentration of residual sulfur ions as a function of reaction time.

14 F. Zhang, H. Yang, X. Xie, L. Li, L. Zhang, J. Yu, H. Zhao and B. Liu, *Sens. Actuators, B*, 2009, **141**, 381.
15 F. Song, H. Su, J. Han, D. Zhang and Z. Chen, *Nanotechnology*, 2009, **20**, 495502.
16 L.-S. Zhong, J.-S. Hu, H.-P. Liang, A.-M. Cao, W.-G. Song and L.-J. Wan, *Adv. Mater.*, 2006, **18**, 2426.
17 M. Cao, T. Liu, S. Gao, G. Sun, X. Wu, C. Hu and Z. Wang, *Angew. Chem., Int. Ed.*, 2005, **44**, 4197.
18 J. Gu, S. Li, E. Wang, Q. Li, G. Sun, R. Xu and H. J. Zhang, *J. Solid State Chem.*, 2009, **182**, 1265.
19 G. Shen, Y. Bando, C. Tang and D. Golberg, *J. Phys. Chem. B*, 2006, **110**, 7199.
20 Y. Huang, K. Yu and Z. Zhu, *Curr. Appl. Phys.*, 2007, **7**, 702.
21 F. Zhou, X. Zhao, C. Yuan and L. Li, *Cryst. Growth Des.*, 2008, **8**, 723.
22 S.-W. Cao, Y.-J. Zhu, M.-Y. Ma, L. Li and L. Zhang, *J. Phys. Chem. C*, 2008, **112**, 1851.
23 R. G. Deshmukh, S. S. Badadhe and I. S. Mulla, *Mater. Res. Bull.*, 2009, **44**, 1179.
24 X. Hu, J. C. Yu and J. Gong, *J. Phys. Chem. C*, 2007, **111**, 11180.
25 B. Hu, S. B. Wang, K. Wang, M. Zhang and S. H. Yu, *J. Phys. Chem. C*, 2008, **112**, 11169.
26 G. Xi, Y. He, Q. Zhang, H. Xiao, X. Wang and C. Wang, *J. Phys. Chem. C*, 2008, **112**, 11645.
27 L. Xu, Y.-S. Ding, C.-H. Chen, L. Zhao, C. Rimkus, R. Joesten and S. L. Suib, *Chem. Mater.*, 2008, **20**, 308.
28 A. L. Washington and G. F. Strouse, II, *J. Am. Chem. Soc.*, 2008, **130**, 8916.
29 X. Cao, C. Zhao, X. Lan, G. Gao, W. Qian and Y. Guo, *J. Phys. Chem. C*, 2007, **111**, 6658.
30 Z. Li, B. Tan, M. Allix, A. I. Cooper and M. J. Rosseinsky, *Small*, 2008, **4**, 231.
31 F. Caruso, M. Spasova, A. Susha, M. Giersig and R. A. Caruso, *Chem. Mater.*, 2001, **13**, 109.
32 T. Hyeon, S. S. Lee, J. Park, Y. Chung and H. B. Na, *J. Am. Chem. Soc.*, 2001, **123**, 12798.
33 S. Yu and M. Yoshimur, *Adv. Funct. Mater.*, 2002, **12**, 9.
34 G. Zou, K. Xiong, C. Jiang, H. Li, T. Li, J. Du and Y. Qian, *J. Phys. Chem. B*, 2005, **109**, 18356.
35 D. Yu, X. Sun, J. Zou, Z. Wang, F. Wang and K. Tang, *J. Phys. Chem. B*, 2006, **110**, 21667.
36 Z. Sun, H. Yuan, Z. Liu, B. Han and Z. Zhang, *Adv. Mater.*, 2005, **17**, 2993.
37 D. Zhang, Z. Liu, S. Han, C. Li, B. Lei, M. P. Stewart, J. M. Tour and C. Zhou, *Nano Lett.*, 2004, **4**, 2151.
38 R. Abu-Reziq, H. Alper, D. Wang and M. L. Post, *J. Am. Chem. Soc.*, 2006, **128**, 5279.
39 G. Lv, F. He, X. Wang, F. Gao, G. Zhang, T. Wang, H. Jiang, C. Wu, D. Guo, X. Li, B. Chen and Z. Gu, *Langmuir*, 2008, **24**, 2151.
40 Z. Liu, J. Wang, D. H. Xie and G. Chen, *Small*, 2008, **4**, 462.
41 A. L. Kohl and F. S. Riesenfeld, *Gas Purification*, Gulf Publishing Co., Houston, 4th edn, 1985, ch. 4, pp. 278–329.
42 B. G. Cox, P. F. Clarke and B. B. Pruden, *Int. J. Hydrogen Energy*, 1998, **23**, 531.
43 L. M. Al-Shamma and S. A. Naman, *Int. J. Hydrogen Energy*, 1989, **14**, 173.
44 F. Bandermann and K. -B. Harder, *Int. J. Hydrogen Energy*, 1982, **7**, 471.
45 M. Yumura and E. Furimsky, *Appl. Catal.*, 1985, **16**, 157.
46 A. Davydov, K. T. Chuang and A. R. Sanger, *J. Phys. Chem. B*, 1998, **102**, 4745.
47 J. Wieckowska, *Catal. Today*, 1995, **24**, 405.
48 L. Zhang, S. Z. Qiao, Y. G. Jin, H. G. Yang, S. Budihartono, F. Stahr, Z. F. Yan, X. L. Wang, Z. P. Hao and G. Q. Lu, *Adv. Funct. Mater.*, 2008, **18**, 3203.

49 M. Mikhaylova, D. K. Kim, C. C. Berry, A. Zagorodni, M. Toprak, A. S. G. Curtis and M. Muhammed, *Chem. Mater.*, 2004, **16**, 2344.
50 T. J. Daou, G. Pourroy, S. Bégin-Colin, J. M. Grenéche, C. Ulhaq-Bouillet, P. Legaré, P. Bernhardt, C. Leuvrey and G. Rogez, *Chem. Mater.*, 2006, **18**, 4399.
51 Y. Lee, J. Lee, C. J. Bae, J.-G. Park, H.-J. Noh, J.-H. Park and T. Hyeon., *Adv. Funct. Mater.*, 2005, **15**, 503.
52 Z. B. Huang, Y. Q. Zhang and F. Q. Tang, *Chem. Commun.*, 2005, 342.
53 A. M. Cao, J. S. Hu, H. P. Liang and L. J. Wan, *Angew. Chem., Int. Ed.*, 2005, **44**, 4391.
54 Y. L. Wang, X. C. Jiang and Y. N. Xia, *J. Am. Chem. Soc.*, 2003, **125**, 16176.
55 X. C. Jiang, Y. L. Wang, T. Herricks and Y. N. Xia, *J. Mater. Chem.*, 2004, **14**, 695.
56 N. Kijima, M. Yoshinaga, J. Awaka and J. Akimoto, *Solid State Ionics*, 2011, **192**, 293.
57 T. Fan, D. Pan and H. Zhang, *Ind. Eng. Chem. Res.*, 2011, **50**, 9009.
58 V. M. Aroutiounian, V. M. Arakelyan, G. E. Shahnazaryan, H. R. Hovhannisyan and J. A. Turner, *Sol. Energy*, 2007, **81**, 1369.
59 M. Zhu and G. Diao, *J. Phys. Chem. C*, 2011, **115**, 18923.
60 E. K. Nyutu, W. C. Conner, S. M. Auerbach, C. -H. Chen and S. L. Suib, *J. Phys. Chem. C*, 2008, **112**, 1407.
61 L. Chen, X. Yang, J. Chen, J. Liu, H. Wu, H. Zhan, C. Liang and M. Wu, *Inorg. Chem.*, 2010, **49**, 8411.
62 X. Su, C. Yu and Qiang, *Appl. Surf. Sci.*, 2011, **257**, 9014.
63 D. L. A. de Faria, S. Venâncio Silva and M. T. de Oliveira, *J. Raman Spectrosc.*, 1997, **28**, 873.
64 N. Pinna, S. Grancharov, P. Beato, P. Bonville, M. Antonietti and M. Niederberger, *Chem. Mater.*, 2005, **17**, 3044.
65 D. Larcher, G. Sudant, R. Patrice and J. M. Tarascon, *Chem. Mater.*, 2003, **15**, 3543.
66 D. Wang, T. Xie and Y. Li, *Nano Res.*, 2009, **2**, 30.
67 X. Hu and J. Yu, *Adv. Funct. Mater.*, 2008, **18**, 880.
68 M. Casula, Y. Jun, D. Zaziski, E. Chan, A. Corrias and A. Alivisatos, *J. Am. Chem. Soc.*, 2006, **128**, 1675.
69 G. Zhang and M. Liu, *J. Mater. Sci.*, 1999, **34**, 3213.
70 C. Chen, Z. Huang, W. Yuan, J. Li, X. Cheng and R. Chi, *CrystEngComm*, 2011, **13**, 1632.
71 Z. Ai, K. Deng, Q. Wan, L. Zhang and S. Lee, *J. Phys. Chem. C*, 2010, **114**, 6237.
72 Y. Cheng, Y. S. Wang, Y. H. Zheng and Y. Qin, *J. Phys. Chem. B*, 2005, **109**, 11548.
73 R. L. Penn, *J. Phys. Chem. B*, 2004, **108**, 12707.
74 J. Park, V. Privman and E. Matijevic, *J. Phys. Chem. B*, 2001, **105**, 11630.
75 Y. Cheng, Y. Wang, D. Chen and F. Bao, *J. Phys. Chem. B*, 2005, **109**, 794.
76 R. L. Penn and J. F. Banfield, *Science*, 1998, **281**, 969.
77 M.-L. Li, Q.-Z. Yao, G.-T. Zhou, X.-F. Qu, C.-F. Mu and S.-Q. Fu, *CrystEngComm*, 2011, **13**, 5936.
78 M.-L. Li, Q.-Z. Yao, G.-T. Zhou and S.-Q. Fu, *CrystEngComm*, 2010, **12**, 3138.
79 G. Sun, B. Dong, M. Cao, B. Wei and C. Hu, *Chem. Mater.*, 2011, **23**, 1587.
80 B. Jia and L. Gao, *J. Phys. Chem. C*, 2008, **112**, 666.
81 K. S. W. Sing, D. H. Everett, R. A. W. Haul, L. Moscou, R. A. Pierotti, J. Rouquerol and T. Siemieniewska, *Pure Appl. Chem.*, 1985, **57**, 603.
82 W. H. Tao and C. H. Tsai, *Sens. Actuators, B*, 2002, **81**, 237.
83 M. A. Sayyadnejad, H. R. Ghaffarian and M. Saeidi, *Int. J. Environ. Sci. Tech.*, 2008, **5**, 565.
84 L. Li and D. L. King, *Catal. Today*, 2006, **116**, 537.
85 M. M. Husein, L. Patruyo, P. Pereira-Almao and N. N. Nassar, *J. Colloid Interface Sci.*, 2010, **342**, 253.